Cell Reports

Report

Differential Mitochondrial Requirements for Radially and Non-radially Migrating Cortical Neurons: Implications for Mitochondrial Disorders

Graphical Abstract

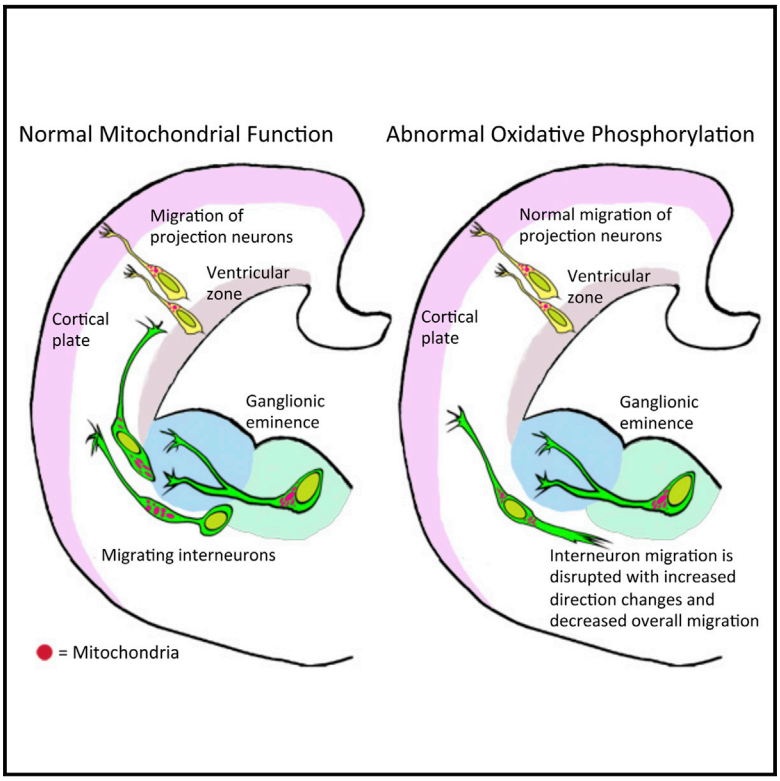

Highlights

- Mitochondria in cortical interneurons are motile during migration
- Mitochondria are stationary in migrating cortical projection neurons
- Oxidative phosphorylation defects disrupt cortical interneuron migration
- Interneurons lose polarity when oxidative phosphorylation is perturbed

Authors

Erika G. Lin-Hendel, Meagan J. McManus, Douglas C. Wallace, Stewart A. Anderson, Jeffrey A. Golden

Correspondence

sande@mail.med.upenn.edu (S.A.A.), jagolden@partners.org (J.A.G.)

In Brief

Mitochondrial disorders frequently result in neurological dysfunction, but the causes of pathogenesis are uncertain. Lin-Hendel et al. show that mitochondrial dysfunction during neurodevelopment selectively disrupts cortical interneuron migration and not projection neuron migration. They further show a specific dependence on oxidative phosphorylation of interneuron migration.

Lin-Hendel et al., 2016, Cell Reports *15*, 229–237
April 12, 2016
http://dx.doi.org/10.1016/j.celrep.2016.03.024

CellPress

Cell Reports
Report

Differential Mitochondrial Requirements for Radially and Non-radially Migrating Cortical Neurons: Implications for Mitochondrial Disorders

Erika G. Lin-Hendel,[1,2] Meagan J. McManus,[3,4] Douglas C. Wallace,[3,4] Stewart A. Anderson,[5,7,*] and Jeffrey A. Golden[6,7,*]
[1]School of Veterinary Medicine, University of Pennsylvania, Philadelphia, PA 19104, USA
[2]Developmental, Regenerative and Stem Cell Biology, Biomedical Graduate Group, University of Pennsylvania, Philadelphia, PA 19104, USA
[3]Center for Mitochondrial and Epigenomic Medicine, Children's Hospital of Philadelphia, Philadelphia, PA 19104, USA
[4]Department of Pathology and Laboratory Medicine, University of Pennsylvania, Philadelphia, PA 19104, USA
[5]Department of Psychiatry, Children's Hospital of Philadelphia, Philadelphia, PA 19104, USA
[6]Department of Pathology, Brigham and Women's Hospital, Harvard Medical School, Boston, MA 02115, USA
[7]Co-senior author
*Correspondence: sande@mail.med.upenn.edu (S.A.A.), jagolden@partners.org (J.A.G.)
http://dx.doi.org/10.1016/j.celrep.2016.03.024

SUMMARY

Mitochondrial dysfunction has been increasingly linked to neurodevelopmental disorders such as intellectual disability, childhood epilepsy, and autism spectrum disorder, conditions also associated with cortical GABAergic interneuron dysfunction. Although interneurons have some of the highest metabolic demands in the postnatal brain, the importance of mitochondria during interneuron development is unknown. We find that interneuron migration from the basal forebrain to the neocortex is highly sensitive to perturbations in oxidative phosphorylation. Both pharmacologic and genetic inhibition of adenine nucleotide transferase 1 (Ant1) disrupts the non-radial migration of interneurons, but not the radial migration of cortical projection neurons. The selective dependence of cortical interneuron migration on oxidative phosphorylation may be a mechanistic pathway upon which multiple developmental and metabolic pathologies converge.

INTRODUCTION

Mitochondrial diseases (MDs) are the most common inherited metabolic disorder, with an estimated prevalence of 1:5,000 (Schaefer et al., 2004). Although MDs consist of a spectrum of disorders that can involve single or multisystem presentations, neurological symptoms are common clinical characteristics. In recent years, clinical, genetic, and biochemical studies have revealed an emerging link between mitochondrial dysfunction and neurodevelopmental disorders, including intellectual disability (ID) (Valenti et al., 2014), childhood epilepsy (Chevallier et al., 2014), and autism spectrum disorder (ASD) (Rossignol and Frye, 2012). Interestingly, these conditions have also been associated with interneuron dysfunction (Marín, 2012). The correlation between MDs and childhood neurological disorders raises the question as to whether interneuron development is particularly dependent on mitochondrial function.

Recent studies have elucidated roles for mitochondria in multiple aspects of neurodevelopment including neuronal differentiation (Wang et al., 2014), process outgrowth (Cheng et al., 2012; Kimura and Murakami, 2014), and synaptogenesis (Bertholet et al., 2013). Most of these studies have utilized glutamatergic hippocampal neurons as a model, leaving the contribution of mitochondria to interneuron development relatively unexplored. Since interneurons are thought to be a key factor in the pathogenesis of epilepsy and ASD, we were particularly interested in examining mitochondrial behavior and function during developmental processes for which there are distinct features between glutamatergic projection neurons (PNs) and GABAergic interneurons (INs) in the cortex. During development, PNs and INs are derived from distinct locations and take different migration routes: PNs migrate along radial glial fibers from their origin in the dorsal ventricular zone and maintain a relatively stable morphology oriented toward the pial surface (Noctor et al., 2004). In contrast, cortical INs take a circuitous path from their origin in the subcortical ganglionic eminences. Along the way, migrating INs frequently pause, change direction, and exhibit extensive branching dynamics of the leading process (Bellion et al., 2005; Lysko et al., 2011, 2014; Polleux et al., 2002).

Given the greater distance and dynamic nature of IN migration, we reasoned that it requires more energy than does the migration of PNs. First, we found that the mitochondria within INs have a highly dynamic localization pattern during non-radial migration. In contrast, mitochondria remain more consistently localized in radially migrating PNs. Second, we found migrating interneurons to be exquisitely sensitive to agents that block the utilization of ATP generated through oxidative phosphorylation. Remarkably, glycolysis alone is insufficient for normal IN migration but is able to support the radial migration of PNs. Moreover, the genetic disruption of mitochondrial oxidative phosphorylation (OXPHOS) in mice lacking *Ant1* was associated with dramatic alterations of IN migratory morphology and behavior, including mispositioning of the centrosomes. Conversely, *Ant1*$^{-/-}$ PNs appeared normal in our migration assays. These data

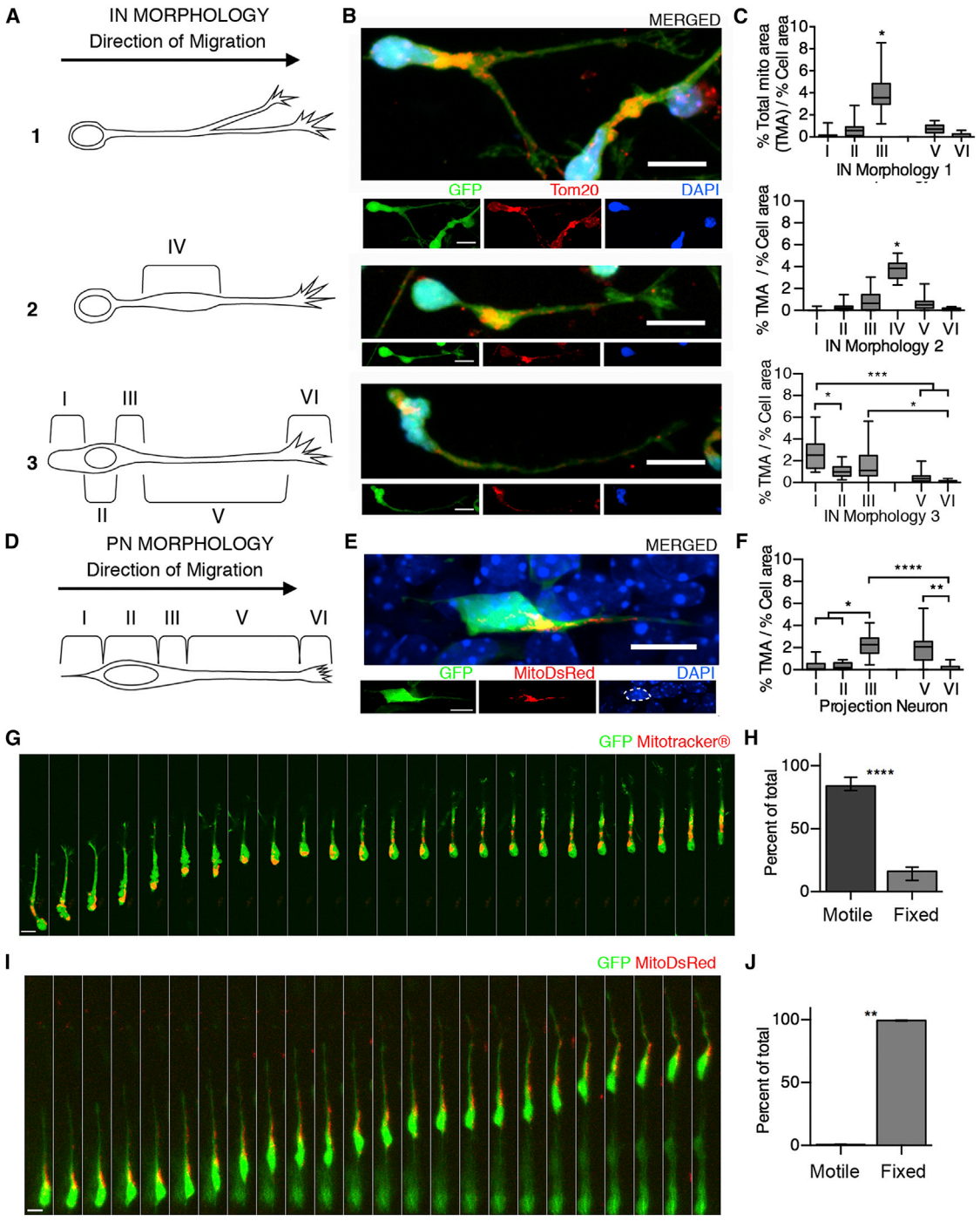

Figure 1. Mitochondrial Localization in Migrating Neurons

(A) Schemata of interneuron (IN; 1–3) morphologies displayed during migration.

(B) Confocal immunofluorescence (IF) images of mitochondria in migrating INs in vitro displaying varying localization patterns according to morphology. Cytosol (GFP), mitochondria (Tom20), and nuclei (DAPI). Scale bar, 10 μm.

(C) Quantification of clustering of mitochondria in subcellular locations. Region I, trailing process (TP); II, overlapping nucleus (Nuc); III, 5 μm anterior to nucleus (5 μm AN); IV, cytoplasmic bleb (bleb); V, leading process (LP); and VI, leading process tip (LPT). Clustering varied markedly between IN morphologies. IN morphology 1 clustered in III (*p = 0.039). IN morphology 2 clustered in IV (*p = 0.02), while IN morphology 3 clustered in I and II (*p = 0.0343 and ***p = 0.0002). Error bars represent median with 25^{th}–75^{th} percentiles ± min/max value of percent total mitochondrial area (%TMA) normalized to region's percent of total cell area (%TCA). n = 15 cells each type; Freidman's test with Dunn's correction.

(D) Schemata of pyramidal neuron (PN) migration morphology.

(legend continued on next page)

suggest that interneuron polarity during migration is particularly sensitive to disruptions in metabolism, and that OXPHOS is required for normal migration of INs but not PNs. Our results also imply that the symptomatic manifestations of mitochondrial dysfunction and related conditions, including hypoxic injury, on cerebral cortical function may be secondary to their selective impact on cortical interneuron migration.

RESULTS

Mitochondria Are Highly Dynamic during Interneuron Migration

To examine the role of mitochondria in non-radial versus radial migration, we first sought to characterize the localization of mitochondria in migrating INs and PNs. We classified medial ganglionic eminence (MGE)-derived cells migrating in explant cultures into three morphological classes corresponding to distinct phases of their migration: leading process extension, forward movement of the centrosome, and nucleokinesis/trailing process retraction (Marín et al., 2006). Morphology 1 cells were defined to have slender, tapered leading processes; morphology 2 cells have a bleb or thickening of the leading process; and morphology 3 cells have a clear trailing process (Figure 1A). Each subgroup displayed a distinct distribution of mitochondria (Figure 1B). In morphology 1, mitochondria were concentrated immediately anterior to the nucleus (Figure 1C; 49 ± 4, % total mitochondrial area [TMA] ± SEM, 5-fold greater % TMA% total cell area [TCA], $p < 0.05$) (Bellion et al., 2005; Golden et al., 1997). In morphology 2 cells, mitochondria were concentrated in the cytoplasmic bleb (Figure 1C; 71 ± 2, %TMA ± SEM, 3.9-fold greater %TMA/%TCA than other areas, $p < 0.05$), while in morphology 3, the mitochondria were aggregated in the trailing process and posterior nuclear area (Figure 1C, 29 ± 4, % TMA ± SEM, 39% ± 5 TMA ± SEM respectively, 1.7-fold greater %TMA/%TCA than other areas, $p < 0.05$) (Bellion et al., 2005).

Although these independent clustering behaviors have been noted in the literature, mitochondrial dynamics during migration have not been studied. To evaluate the subcellular localization of mitochondria in relation to the morphological migratory phases, we next performed time-lapse imaging of fluorescently labeled mitochondria in migrating interneurons. Interestingly, mitochondria displayed consistent positional reorganization during migration, as their subcellular location changed in concert with the morphology of the migrating cell (Figures 1G and 1H; Movie S1). The mitochondrial localization and changes in location observed in the three IN morphologies were confirmed by live imaging of mitochondria in whole-brain-slice cultures from embryonic day 13.5 (E13.5) embryos (Figure S1; Movie S2). The localization of mitochondria in migrating INs was ranked according to morphology as matching or not matching the localization observed in migrating dissociated INs and found to be highly correlated (Figure S1A).

In contrast to migrating INs, migrating PNs maintain a relatively consistent migratory morphology after leaving their multipolar phase in the ventricular and subventricular zones (Figure 1D and 1I) (Noctor et al., 2004). During radial migration in the cortical plate, mitochondria were found primarily anterior to the nucleus and in the leading process, showing little change in regional localization (Figures 1E, 1F, 1I, and 1J; Movie S3). These data reveal that the intracellular position, and changes in location, of mitochondrial of INs and PNs are clearly distinguishable and suggest that there may be differences in energy requirements between these two neuronal cell populations during development.

Oxidative Phosphorylation Is Necessary for Normal IN Migration, but Not for Radial Migration

To determine whether migrating INs and PNs have distinct energetic requirements, we studied their need for mitochondrially generated ATP in explant and slice cultures. Cells generate ATP through glycolysis in the cytosol and oxidative phosphorylation (OXPHOS) in the mitochondria. To test whether OXPHOS is necessary for normal neuronal migration, we examined cell movement after blocking OXPHOS with either oligomycin or bongkrekic acid (BA). Oligomycin (Olig) blocks mitochondrial production of ATP by inhibiting the ATP synthase (Kulka and Cooper, 1962), while BA prevents the translocation of ATP across the inner mitochondrial membrane by inhibiting the adenine nucleotide translocator isoforms 1 (*Ant1*, also known as *Slc25a4*) and 2 (*Ant2* also known as *Slc25a5*) (Henderson and Lardy, 1970). IN migration was exquisitely sensitive to Olig treatment, where 0.02 μM reduced IN migration by 78% (Figure S2A; Movie S4). Treating INs with 2.5 μM BA reduced IN migration by 50% ($p \leq 0.001$) (Figure 2A; Movie S5). These cells showed no reduction in somal translocation (Figure 2C; not statistically significant but trending toward slower) but a significant increase in the time spent paused (Figure 2D). Interestingly, treated cells exhibited elongated trailing processes (Figures 2B and 2F) as well as a higher frequency of trailing processes (Figure 2E) and for more time (Figure 2G) than controls. Furthermore, at low BA concentrations, migrating INs exhibit a 10-fold increase in direction changes (Figure 2H). BA also resulted in significant reduction in the leading process length (Figure 2I). The

(E) Confocal IF images of mitochondria in representative migrating PN. Cytosol (GFP), mitochondria (MitoDsRed), and nuclei (DAPI). Scale bar, 10 μm.

(F) Quantification of clustering mitochondria in migrating PNs. Region I: TP; II: Nuc; III: 5 μm AN; IV: cytoplasmic bleb (bleb); V: LP; VI: leading process tip LPT. *p = 0.0327, **p = 0.0064, and ****p < 0.0001. n = 15 cells; Freidman's test with Dunn's correction.

(G) Time-lapse imaging of a migrating *Dlx5/6*^{CIG} IN in vitro (cytosol, GFP; mitochondria, MitoTracker Red CMXRos) show intracellular movement of mitochondria. 1 frame = 10 min. Scale bar, 10 μm. See also Movie S2.

(H) Quantification of INs displaying a extensive movement of mitochondrial through the cell versus those where the mitochondria remain confined to one compartment. The majority of INs showed this movement of mitochondria throughout the cell during migration. $p < 0.0001$, unpaired t test, n = 5 independent cultures, 200 cells. Values represent mean ± SEM.

(I) Live time-lapse imaging of a migrating PN (cytosol, GFP; mitochondria, MitoDsRed). 1 frame = 10 min. Scale bar, 10 μm. See also Movie S3.

(J) Quantification of PNs movement of mitochondrial through the cell versus those where the mitochondria remain confined to one compartment. Intracellular movement of mitochondria through PNs was essentially not observed. p = 0.002, Mann-Whitney, n = 6 independent cultures, 82 cells. Values represent mean ± SEM.

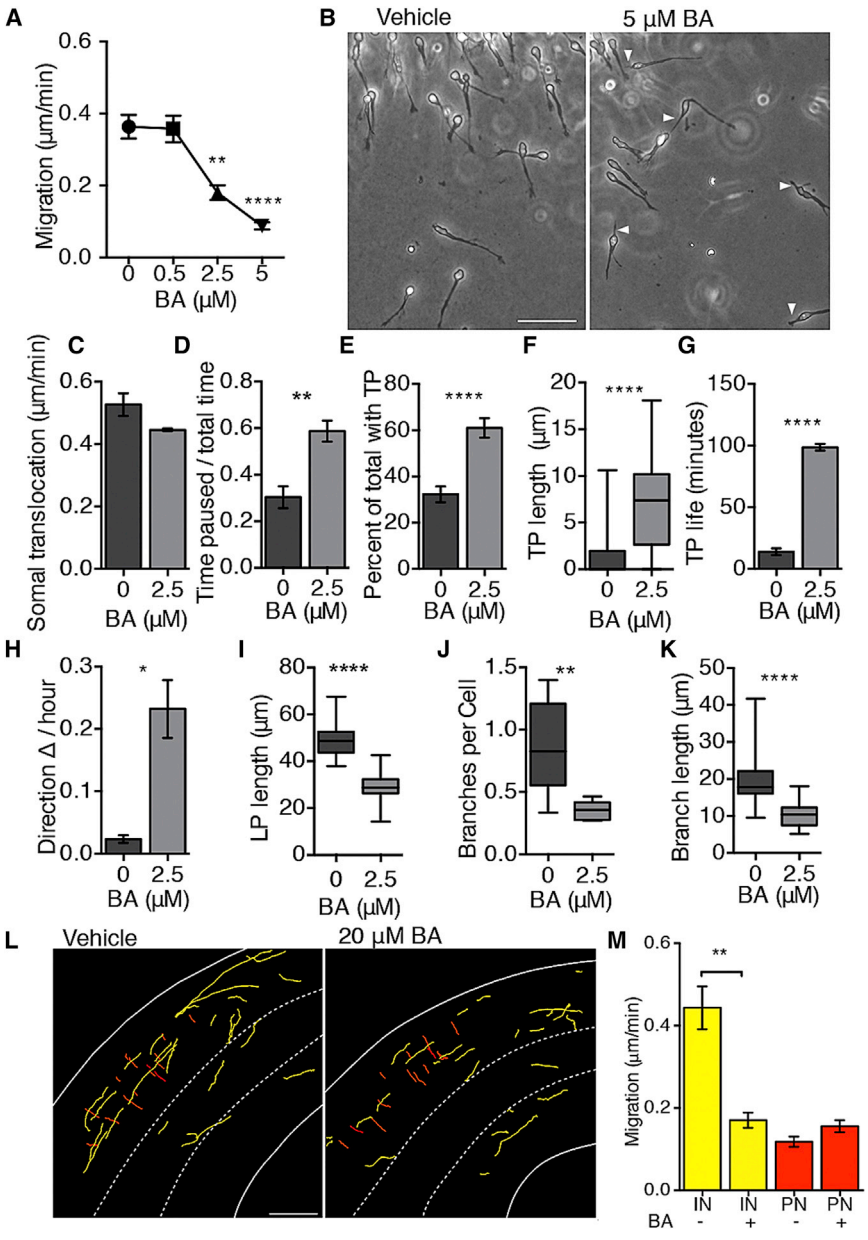

Figure 2. Pharmacological Inhibition of OXPHOS Reduces IN Migration

(A) MGE explants were cultured in high glucose ± BA, an inhibitor of OXPHOS. Inhibiting OXPHOS decreased IN migration. (BA concentration: 0 μM and 0.5 μM = 0.36 ± 0.4; 2.5 μM = 0.18 ± 0.02, 5 μM = 0.09 ± 0.01; all in μm/min ± SEM; 0 versus 2.5 or 5, $p \leq 0.001$, n = 5 independent cultures, >150 cells each, ANOVA test).

(B) Representative phase image of BA-treated MGE INs. Arrows identify elongated trailing processes. Scale bar, 50 μm.

(C) Somal translocation was calculated for each migrating IN; while slightly slower, this did not reach significance (BA concentration: 0 μM = 0.53 ± 0.04; 2.5 μM = 0.45 ± 0.01; all in μm/min ± SEM; $p \leq 0.075$, n = 5 independent cultures, > 150 cells each, unpaired t test, Welch's correction).

(D) The time a migrating neuron was paused versus moving was also calculated. In the presence of BA, the neurons spend significantly more time paused compared to control cells (BA concentration: 0 μM = 0.30 ± 0.05; 2.5 μM = 0.59 ± 0.05; all in total time paused/imaging period ± SEM; $p \leq 0.002$, n = 5 independent cultures, > 150 cells each, unpaired t test, Welch's correction).

(E–G) In addition to decreased migration, inhibition of OXPHOS increased the frequency (E; $p < 0.001$, unpaired t test with Welch's correction, mean ± SEM), length (F; $p < 0.0001$, Mann Whitney, median with interquartile range ± min/max), and life of trailing processes (G; $p < 0.0001$, Mann-Whitney). For each, n = 5 independent cultures, 100 cells each.

(H) OXPHOS inhibition also causes increases in direction changes (the mean number of direction changes/hour ± SEM was 0.024 ± 0.006 for 0 μM BA; and 0.23 ± 0.05 for 2.5 μM BA, $p < 0.0001$; n = 5 independent cultures, 100 cells each, unpaired t test with Welch's correction).

(I–K) Leading process length (I), branches/cell (J), and branch length (K) were all significantly reduced in migrating INs treated with BA when compared to controls ($p < 0.0001$, $p < 0.001$, and $p < 0.0001$, respectively, Mann-Whitney test).

(L) Sample migration paths of INs (yellow) and PNs (red) in E16 brain slices treated with vehicle or 20 μM BA. See also Movie S5. CP, cortical plate; IZ, intermediate zone; VZ, ventricular zone. Scale bar, 150 μm.

(M) IN migration rates decreased in slices treated with BA ($p = 0.0023$, n = 6 individuals, 20 INs each) whereas PNs were unaffected ($p > 0.05$, n = 6 individuals, ≥ 15 PNs in each). Unpaired t test with Welch's correction, mean ± SEM.

leading processes also branched less frequently and the branch lengths were significantly reduced (Figures 2J and 2K).

To determine whether OXPHOS is sufficient to supply energy for IN migration, we removed glucose (GLUC) from the medium or inhibited glycolysis with 2-deoxyglucose (2-DG) and provided the OXPHOS substrate pyruvate (PYR). Alternatively, we substituted GLUC for galactose (GAL). GLUC deprivation reduced migration by ~53% (Figure S2C), while inhibition with 2-DG reduced migration by ~68% (Figure S2C). When INs are supplemented with PYR or GAL, ATP generation is dependent on OXPHOS alone (Adeva-Andany et al., 2014; Marroquin et al., 2007). Both PYR and GAL were sufficient to fully rescue IN migration under conditions of glycolysis inhibition, and this ability to sustain migration was abrogated with addition of subthreshold doses of BA (Figure S2C). Therefore, OXPHOS is both necessary and sufficient for normal IN migration.

The requirement for OXPHOS in neuronal migration was further tested using slice cultures where both non-radially migrating INs, and radially migrating PNs, could be studied simultaneously. We utilized *Dlx5/6*^{CIG} mice in which the INs are genetically labeled with EGFP. At E14, a DsRed expression construct was electroporated into *Dlx5/6*^{CIG} embryos to label

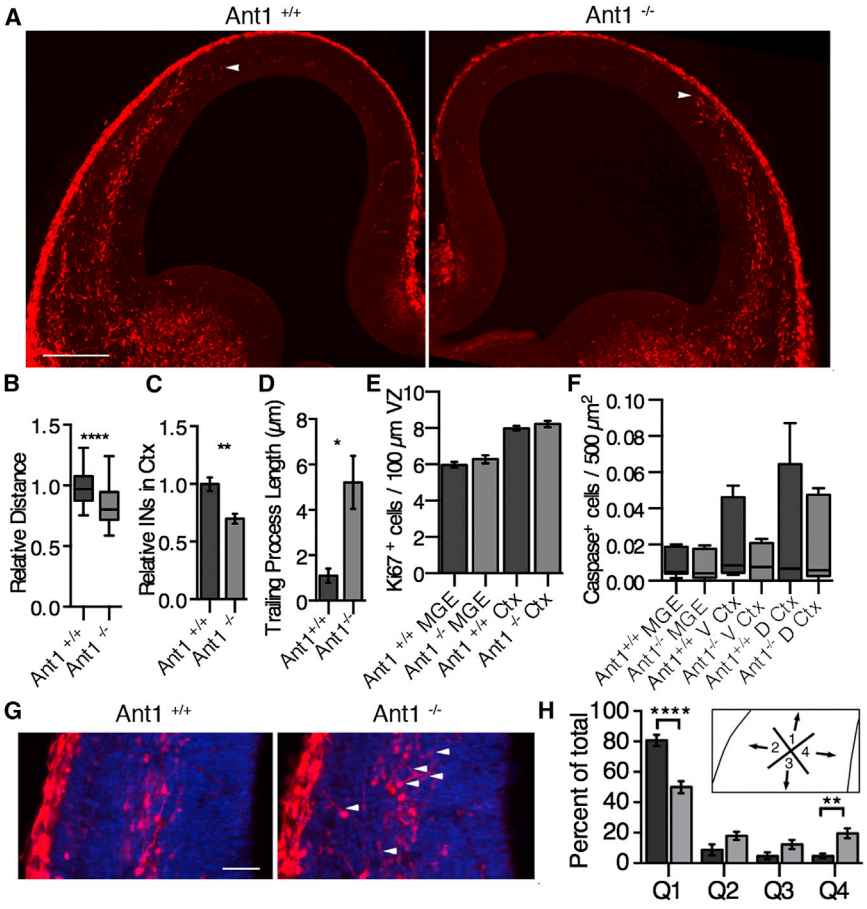

Figure 3. Interneuron Migration Is Reduced in Embryonic *Ant1* Mutants

(A) At E13.5 migrating INs (labeled by calbindin immunohistochemistry) have not traveled as far in *Ant1*$^{-/-}$ brains compared to *Ant*$^{+/+}$ brains. The white arrow indicates the leading migrating INs. *Ant1*$^{+/+}$ served as the standardized control distance of 1.0 ± 0.02 with *Ant1*$^{-/-}$ IN migration showing on average 0.85 ± 0.02 relative distance units ± SEM or a 15% reduction, $p < 0.0001$. Scale bar, 200 μm.

(B) Quantification of relative distance of leading cells of migrating INs. ****$p < 0.0001$, n = 5 individuals, 25 cells each, Mann-Whitney test. Values represent median with interquartile range ± min/max.

(C) Quantification of relative INs in cortex ; *Ant1*$^{+/+}$ = 1.0 ± 0.06; *Ant1*$^{-/-}$ = 0.7 ± 0.04; normalized INs in cortex ± SEM, **$p = 0.004$, n = 5, unpaired t test with Welch's correction.

(D) *Ant1*$^{-/-}$ INs in the cortex have increased trailing process (TP) length. *Ant1*$^{+/+}$: 1.1 μm ± 0.3; *Ant1*$^{-/-}$: 5.2 μm ± 1.1 (±SEM), *$p = 0.022$, n = 5 individuals, 25 cells each, unpaired t test with Welch's correction.

(E) Proliferation in germinal ventricular zone (VZ), indicated by Ki67 immunostaining, was not impacted by loss of *Ant1*. Medial ganglionic eminence (MGE) and pallium (Ctx). *Ant1*$^{+/+}$ versus *Ant1*$^{-/-}$ for each region, $p = 0.286$ for MGE, $p = 0.309$ for Ctx; n = 5 individuals, unpaired t test with Welch's correction.

(F) Loss of Ant1 did not increase cell death, indicated by caspase-3, in the MGE and the ventral and dorsal pallium (V/D Ctx). *Ant1*$^{+/+}$ versus *Ant1*$^{-/-}$ for each region, $p > 0.99$, n = 5 individuals, Kruskal-Wallis, Dunn's correction. Values represent median, 25th–75th percentile ± min/max.

(G) INs in cortex of *Ant1*$^{-/-}$ mice displayed abnormal leading process orientation. Arrowheads indicate misaligned INs. Scale bar, 75μm.

(H) Quantification of cortical IN leading process orientation into quadrants: Q1, dorsal; Q2, pial; Q3, ventral; and Q4, ventricular orientation. The average percent of IN oriented in Q1 for *Ant1*$^{+/+}$ was 80 ± 4 and 50 ± 4; *Ant1*$^{-/-}$ (±SEM), ****$p = 0.0001$ and **$p = 0.0069$, n = 5, ANOVA with Sidak's correction.

the progenitors of radially migrating PNs. Embryos were harvested at E16, and cortical slices from individuals were treated with BA. Remarkably, BA treatment reduced IN migration rates, whereas PNs were unaffected (Figures 2L and 2M; Movie S6; IN: 0.289 ± 0.06 μm/min decrease, $p < 0.002$; PN: 0.03 ± 0.02 μm/min increase, $p > 0.1$). These data demonstrate that the non-radial migration of cortical interneurons is dependent on OXPHOS, while the radial migration of cortical projection neurons is either not or minimally OXPHOS dependent.

Selective Disruption of Non-radial IN Migration in *Ant 1*$^{-/-}$ Mutants

We next sought to corroborate our pharmacologic data of the differential effects of OXPHOS on PN versus IN migration in mice lacking the *Ant1* isoform. The genetic removal of *Ant1* reduces the ATP flux from the mitochondria to the cytosol, and *Ant1* is expressed in cortical neurons, including INs (Figures S3A and S3B; Graham et al., 1997; Lee et al., 2009; Levy et al., 2000).

To determine if loss of *Ant1* disrupts IN migration in vivo, *Ant1*$^{+/+}$ and *Ant1*$^{-/-}$ brains were sectioned and stained for calbindin at E13.5 to detect a subset of migrating INs. On average, the leading edge of INs from wild-type brains migrated 15% percent farther than that of *Ant1*$^{-/-}$ brains (Figures 3A and 3B), and there was a 30% decrease in total migrating INs invading the cortex in *Ant1*$^{-/-}$ animals (Figure 3C). Additionally, *Ant1*$^{-/-}$ migrating INs displayed aberrant orientation of the leading process with 30% fewer cells oriented in the main migration path (Figures 3G and 3H). Interestingly, *Ant1*$^{-/-}$ INs had longer trailing processes in vivo (Figure 3D), a characteristic also seen in wild-type INs treated with BA in vitro (Figure 2C). Neither proliferation nor cell death in the MGE or cortex was impacted by loss of *Ant1*$^{-/-}$ (Figures 3E and 3F), excluding these mechanisms as an explanation for the reduction of cells in the mutant cortex. This suggests that a migration phenotype is the primary cause for the IN defect in *Ant1*$^{-/-}$ embryonic cortex.

To confirm the effect of *Ant1* deficiency on IN migration, *Ant1*$^{-/-}$ MGE explants were assayed. *Ant1*$^{-/-}$ INs migrated shorter distances (~40% decrease; Figures 4A and 4B), and more slowly (~42% decrease; Figure 4C) when compared to *Ant1*$^{+/+}$ INs. Interestingly, *Ant1*$^{-/-}$ IN migration was exquisitely sensitive to BA treatment, showing large reductions in IN migration rates at doses that had no effect on *Ant1*$^{+/+}$ cells (Figures 4C), likely due to further blocking of mitochondrial ATP efflux through inhibition of the *Ant2* isoform (Graham et al., 1997; Levy et al., 2000).

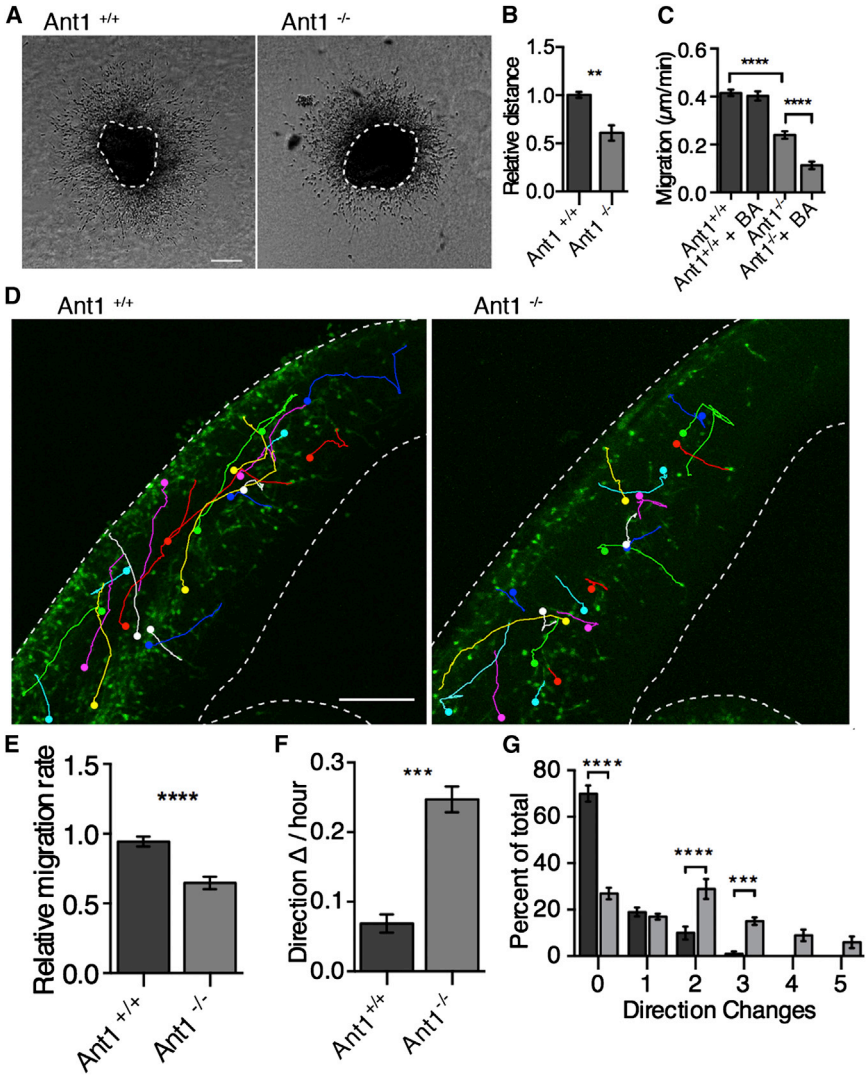

Figure 4. Abnormal Migration by *Ant1*$^{-/-}$ Interneurons

(A) MGE explants were cultured in vitro for 16 hr. *Ant1*$^{-/-}$ INs did not migrate out of the explant as far as controls.

(B) Quantification of relative distance of IN migration from explant showing a statistically significant difference in the distance migrated between *Ant1*$^{-/-}$ and *Ant1*$^{-/-}$ INs., *Ant1*$^{+/+}$ is calculated as the normalized distance (1.0 ± 0.03) and *Ant1*$^{-/-}$ was on average approximately 40% reduced (0.61 ± 0.08); normalized distance ± SEM. **p = 0.0034, n = 6, 50 cells each genotype, unpaired t test with Welch's correction. Scale bar, 250 μm.

(C) Quantification of IN migration rates of wild-type and mutant INs. *Ant1*$^{-/-}$ IN migration rates had slower migration rates (****p < 0.0001) and were more sensitive to BA treatment compared to *Ant1*$^{+/+}$(****p < 0.001). Migration rates *Ant1*$^{+/+}$: 0.42 ± 0.01; *Ant1*$^{-/-}$: 0.24 ± 0.01; μm ± SEM, n = 5, 150 cells each condition, ANOVA with Bonferonni's correction.

(D) Examples of migration path of GFP^{+} INs in slice culture (also see Movie S7). Dots, start; lines, paths. Scale bars, 150 μm.

(E) *Ant1*$^{-/-}$ INs in slices display decreased migration rates relative to control. The relative migration rate was compared between Ant1$^{+/+}$: 0.94 ± 0.04 and Ant1$^{-/-}$: 0.65 ± 0.04; relative migration rate ± SEM, ****p < 0.0001, n = 5, unpaired t test with Welch's correction.

(F) *Ant1*$^{-/-}$ INs display increased direction changes. Ant1$^{+/+}$: 0.07 ± 0.01; Ant1$^{-/-}$: 0.25 ± 0.02; direction changes per cell/hr ± SEM, p < 0.0001, n = 5, unpaired t test with Welch's correction.

(G) Frequency plot of IN direction changes; dark gray = *Ant1*$^{+/+}$, light gray = *Ant1*$^{-/-}$. ****p < 0.0001 and ***p = 0.0006, n = 5, two-way ANOVA with Sidak's correction.

In contrast to the clear defects in IN migration, *Ant1*$^{-/-}$ PN migration was normal. E14.5 embryos were electroporated with pCAG-IG and cell positions assayed on E18.5. The loss of *Ant1* did not alter radial migration (Figures S3A and S3B). To further assay the migration of PNs, we injected 5-ethynyl-2'-deoxyuridine (EdU) to pregnant dams on E14.5 and harvested the embryos on E18.5. Labeling for EdU (E14.5 injections mainly label outer layer neurons) and Tbr1 (a deeper layer neuronal marker) showed normal positioning of cortical neurons between *Ant1*$^{+/+}$ and *Ant1*$^{-/-}$ brains (Figure S4C). Together, these data indicate that in marked contrast to the non-radial migration of cortical INs, Ant1 does not appear to affect the radial migration of PNs.

Loss of *Ant1* Alters Centrosome Localization in Migrating Interneurons

To further examine the migration behaviors disrupting IN migration in *Ant1*$^{-/-}$ mutants, we crossed these mice to *Dlx5/6*^{CIG} mice to genetically label forebrain GABAergic neurons. Live imaging of slices from *Ant1*$^{-/-}$ and littermate *Ant1*$^{+/+}$ controls revealed an ~31% decrease in migration rates of GFP^{+} cells in the cortex (Figure 4E) and ~3.6-fold increases in direction changes (Figures 4D, 4F, and 4G; see also Movie S7). These data suggest an impaired ability of *Ant1*$^{-/-}$ INs to maintain polarity. To study this further, we examined centrosome localization in MGE explant cultures. In control INs, the centrosome localizes anterior to the nucleus or in the bleb of the leading process. *Ant1*$^{-/-}$ INs displayed markedly aberrant centrosome positions, posterior to the leading edge of the nucleus, or even behind the nucleus (Figures 5A and 5B). To confirm this finding, we also assayed the localization of centrosome after BA. Similar to the findings in the *Ant1*$^{-/-}$, BA-treated migrating INs also displayed a significant posterior positioning of the centrosome (Figures 5C and 5D). Taken together with the increased direction changes seen after either genetic or biochemical impairment in mitochondrial energetics, these results suggest that IN polarity is particularly sensitive to mitochondrial perturbation.

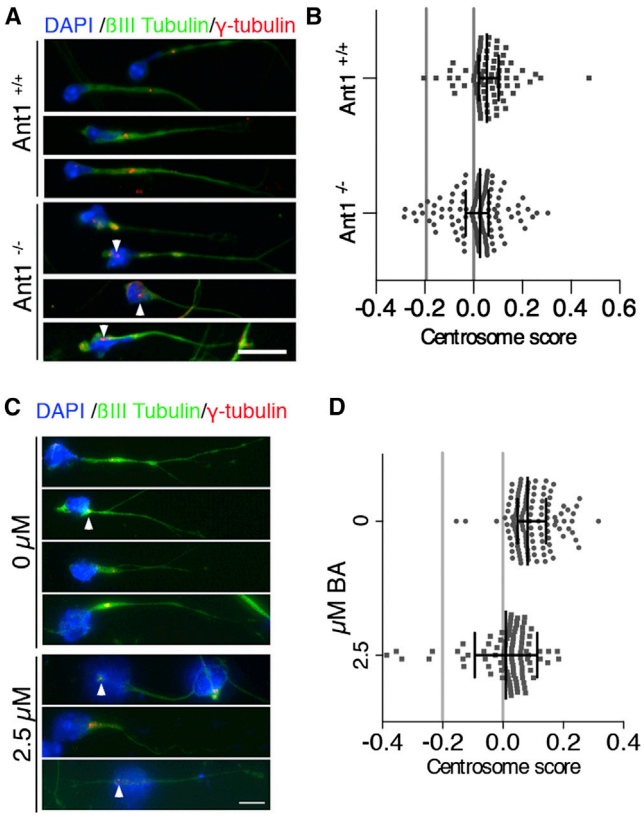

Figure 5. Loss of Ant1 Causes a Shift in Centrosome Position

(A and C) Sample images of centrosome position in INs show mislocalized centrosome in Ant$^{-/-}$ INs (A) and BA-treated INs (C) in vitro. Gamma-tubulin, red; nucleus, blue; cytoplasm, green. Scale bar, 15 μm.

(B and D) Scatterplot of centrosome score of Ant$^{-/-}$ (B) and BA-treated (D) INs (gray lines, average nuclear length). Ant1$^{+/+}$: 0.06 ± 0.01; Ant1$^{-/-}$: 0.02 ± 0.01; centrosome score ± SEM; p = 0.0005, n = 75 cells each genotype, Mann-Whitney test, median with interquartile range ± min/max.

DISCUSSION

Our results reveal that migrating INs and PNs display major differences in mitochondrial localization. During IN migration, mitochondrial localization is highly dynamic, with the highest density of mitochondria appearing to move between the posterior trailing process, the region anterior to the nucleus, and the cytoplasmic bleb. In contrast, during PN migration, mitochondria are primarily restricted to the region anterior to the nucleus. We also found that inhibition of OXPHOS drastically decreased the migration rates of INs, but not PNs. These findings suggest that INs, unlike radially migrating PNs, are highly dependent on mitochondrial ATP production. The reduced migratory rates and increased direction changes by INs also suggest that the maintenance of polarity is an energetically vulnerable process and is required for normal IN development. These data link mitochondrial function to the prenatal development of a critical cerebral cortical neuronal subpopulation.

Few studies have addressed mitochondrial localization and trafficking in migrating neurons. Previous work has shown that Lis1, Tau 1, and DCX, genes that cause defects in radial migration and IN development, cause mislocalized and altered mitochondrial trafficking (Khalaf-Nazzal et al., 2013; Sapir et al., 2012; Yamada et al., 2009). Although this suggests that defects in mitochondrial localization may also impact PNs, each of these genes also regulates microtubule dynamics. Thus, in these models, it is unclear whether changes in mitochondrial localization contribute to the defects in radial migration or whether these genes have a direct impact on mitochondrial function. Our data address this issue by investigating mitochondrial localization in both PN and IN populations and by interfering directly with mitochondrial function. Although mitochondrial dysfunction in addition to other defects may contribute to abnormal radial migration, we provide clear evidence that INs are much more sensitive to OXPHOS deficits.

Mitochondrial contribution to neuronal metabolism has been largely studied in the context of the adult nervous system, focused on how loss of mitochondrial function results in neurodegeneration and cell death. Recent data have emphasized the importance of mitochondrial energetics in basic neurophysiology. For example, mitochondrial energetics are essential for interneuron regulation of gamma oscillations that are themselves associated with cognitive functions (Kann et al., 2014). However, few data exist on the earlier developmental requirements for mitochondrial OXPHOS. Several studies have indicated that regulation of mitochondrial metabolism impacts neurogenesis and differentiation (Bertholet et al., 2013; Wang et al., 2014), but the requirement for OXPHOS during neuronal migration had not been studied. Surin et al. suggested that glycolysis is a primary driver of embryonic neuronal metabolism of hippocampal cultures (Surin et al., 2012). Since interneurons comprise only ~6% of the neurons in hippocampal cultures (Benson et al., 1994), it is likely the measurements in this study were primarily representative of pyramidal neuron metabolism. This lack of active OXPHOS in embryonic pyramidal cells thus compliments our findings that PN migration is not impacted by OXPHOS inhibition. Our data clearly show that interneuron migration required OXPHOS and suggest that distinct neuronal populations have different metabolic requirements during development.

We found that *Ant1* mutant INs exhibit changes in centrosome localization, increased length of the trailing process, and increased direction changes during IN migration. Mitochondria have been implicated in centrosome homeostasis in mitotic cells (Donthamsetty et al., 2014). Additionally, the mislocalization of centrosomes has also been observed in mice lacking mDia1 and 3, proteins of the formin family that regulate cytoskeletal dynamics via Rho-GTPases (Daou et al., 2014). Interestingly, IN migration is disrupted in these mutants, but radial migration is not (Shinohara et al., 2012). In this model, focus was on subventricular zone migration of interneurons to the olfactory bulb; thus, it is unclear whether there are additional phenotypic similarities exist between these models. The similarities in our phenotype and selective effect on INs suggest that the regulation of centrosomal position and actinomycin contractions within the trailing process are energetically vulnerable processes and warrant further investigation.

Patients with ASD, and particularly those with combined ASD, ID, and epilepsy, commonly have evidence of mitochondrial dysfunction (Rossignol and Frye, 2012). The manner by which

mitochondrial dysfunction contributes to these phenotypes is generally attributed to a deficiency in meeting ongoing neuronal metabolic demands or increased free radical production resulting in cell death. Our data provide clear evidence for a final common pathway into the pathogenesis of ASD, developmental epilepsies, and IDs. These clinical phenotypes associated with mitochondrial disorders may not solely arise from energetic deficits or the formation of free radicals during later neuronal function but may be secondary to abnormal IN development.

EXPERIMENTAL PROCEDURES

Mouse Strains

CD1 or *Dlx5/6*^{CIG} (Stenman et al., 2003) and *Ant1*$^{-/-}$ mice on a C57BL6/NJ (Ronchi et al., 2013) of both sexes were used as indicated. The Institutional Animal Care and Use Committee at the Children's Hospital of Philadelphia (Philadelphia, PA) approved all studies.

Brain Explant and Slice Cultures

Explant and slice cultures were generated from the indicated embryonic day mouse pups as previously described (Lysko et al., 2011, 2014).

Treatment Protocols

For inhibition of oxidative phosphorylation, explants were cultured for 24 hr in Dulbecco's media (DM) with 35 mM glucose. Immediately prior to imaging, media was exchanged with DM with PBS vehicle, Oligo (Sigma), or BA (Enzo Life Sciences). We found a strain difference in response to treatment to BA. CD1 cells were treated with 0.5, 2.5, 5, and 50 μM BA, while *Ant1*$^{+/+}$ and *Ant1*$^{-/-}$ cells were treated with 0.5 fM BA. For glucose deprivation and inhibition experiments, explants were cultured for 24 hr in glucose-free DMEM (Invitrogen) plus N2 supplement (Gibco) with or without 10 mM sodium pyruvate (Sigma) or 5 mM galactose (Sigma), ± 2.5 μM BA. For treatment with 2-DG, explants were cultured for 24 hr with 5 mM glucose DM supplemented with 500 μM 2-DG (Sigma), with or without 10 mM sodium pyruvate or 5 mM galactose ± 0.5 μM BA.

Histology and Immunocytochemistry

Brains of E13.5, E16, or E18.5 embryos were processed for histology and immunohistochemistry as previously described (Lysko et al., 2011). Primary antibodies used included anti-calbindin D-28k (rabbit; Swant, 1:1,000), caspase-3 (rabbit; Abcam, 1:500), Ki67 (rabbit; Neomarkers, 1:300), anti-Tom-20 (rabbit; Santa Cruz Biotechnology, 1:500), and anti-GFP (chicken: Invitrogen, 1:2,000). Secondary antibodies included goat anti-rabbit-biotin (Vector Laboratories) followed by Streptavidin/Alexa Fluor 594 (Invitrogen) or anti-rabbit-Alexa Fluor 594 (Invitrogen) anti-chick-Alexa 488 (Invitrogen), all at 1:2,000. Nuclei were counterstained with DAPI.

MGE explants were fixed and immunolabeled as previously described (Lysko et al., 2011, 2014) using anti-Tuj1 (rabbit; Neuronal CIII b-tubulin; Covance, 1:1,000), anti gamma-tubulin (mouse; Sigma, 1:200), anti-GFP (chicken; Invitrogen, 1:200), or anti-Ant1 (rabbit) as primary antibodies.

Intrauterine Electroporations

Embryos at either E14 or E14.5 were electroporated in utero as previously described (Nasrallah et al., 2012) with the following constructs: pCAG-IG (Addgene 11150; 2 μg/μl), pCAG-DsRed (Addgene 11151; 2 μg/μl), pDsRed2-mito (MitoDsRed; Clontech 632421; 0.5 μg/μl). For marking mitochondria in radially migrating neurons and slice BA treatments, embryos were electroporated at E14 and harvested 48 hr later. For assessing radial migration, embryos were electroporated at E14.5 and harvested at E18.5.

Live Marking of Mitochondria In Vitro

To image mitochondria in migrating INs, explants from *Dlx5/6*^{CIG} embryos were cultured for 24 hr. Prior to imaging, cells were treated with 100 nM MitoTracker Red CMXRos (Invitrogen) for 30 min in Opti-MEM (Invitrogen) with 10 mM glucose. Cells were then rinsed with PBS and supplied with fresh DM before imaging.

Microscopy

For all experiments, time-lapse images were acquired at indicated intervals for a minimum of 6 hr with an Olympus Fluoview (FV10i) confocal microscope at 37°C, 5% CO^2. Magnifications were as follows: 10× magnification with 2× zoom for treatment protocols at 5-min intervals, and 10× magnification in slices at 10-min intervals. For higher resolution, 60× magnification was used for acquiring mitochondrial localization in migration INs at 10-min intervals. For slices, z stacks of 10 μm each were taken, capturing the full range of detectable GFP$^+$ cells or DsRed cells within the slice. Slices were imaged for a minimum of 5 hr. Images of fixed explants cells and slices were taken on an Olympus Fluoview (FV10i) confocal microscope at 20× magnification. Mitochondria were localized within individual cells from 40-μm floating brain slices by collecting 1.5-μm z stacks in using the Olympus Fluoview (FV10i) confocal microscope at 60× magnification. Mitochondria were labeled with Tom20, and EGFP, driven by the Dlx5/6 promoter, was detected with the anti-GFP antibody. Images of calbindin-stained slices and were taken at 5× and 10× magnification every 5 μm for 15 μm on a Leica CTR600 fluorescent microscope.

Quantification

In all experiments, cells were selected at random using ImageJ's grid plugin for all experiments unless indicated otherwise. The color-profiler ImageJ plugin was used to generate plots of fluorescence units. For fixed cells, mitochondrial area was calculated by thresholding images using ImageJ's auto-local thresholding plugin (for invitro culture, Bernsen method, 15 pixels) or by color thresholding images for overlapping green and red pixels (for cells in fixed slices). Thresholded images were analyzed using the particle analyzer plugin to calculate mitochondrial area in subcellular regions. Distance of migration along the cortex of the 25 leading cells was measured as a percentage of the distance between the striatocortical notch and dorsal cortical curve and normalized to the average distance of wild-type littermates. Relative migration distance for explants was calculated from the explant edge to the position of the ten cells that had migrated the furthest. Values were normalized to averages of *Ant1*$^{+/+}$ littermates. Cell migration speed was calculated as previously published (Lysko et al., 2011). Leading process orientation was calculated by designating cells into quadrants based on the orientation of their leading processes. Centrosome scores were determined by defining the anterior edge of the nucleus as zero and centrosomes positioned behind the leading edge of the nucleus as negative values. Centrosome position was measured from the posterior of the cell and represented as a percent of total cell length.

Statistics

Prism 6 software was used for all statistical analysis. Data were tested for normality using either the Kolmogorov-Smirnov test or the D'Agostino and Pearson omnibus normality test. If the data were not normal, non-parametric analysis was utilized. $p < 0.05$ were considered significant. All values are presented as mean ± SEM unless otherwise indicated.

SUPPLEMENTAL INFORMATION

Supplemental Information includes Supplemental Experimental Procedures, four figures, and seven movies and can be found with this article online at http://dx.doi.org/10.1016/j.celrep.2016.03.024.

AUTHOR CONTRIBUTIONS

E.G.L. collected data, processed, and performed analysis. E.G.L., J.A.G., and S.A.A. contributed to experimental design and wrote the paper. J.A.G. and S.A.A. contributed equally to the design, execution and interpretation of all studies. D.C.W. and M.J.N. contributed to pharmacological study design and experimental interpretation. All authors discussed the results and commented on the manuscript.

ACKNOWLEDGMENTS

This work was supported in part by NIH grants NS21328, NS41850, NS070298 (to D.C.W.), NS46166 (to J.A.G.), Simons Foundation Grant 205844 (to D.C.W.), and by the RAF Penrose Endowed Chair (to S.A.A.).

Received: January 12, 2015
Revised: February 8, 2016
Accepted: March 4, 2016
Published: March 31, 2016

REFERENCES

Adeva-Andany, M., López-Ojén, M., Funcasta-Calderón, R., Ameneiros-Rodríguez, E., Donapetry-García, C., Vila-Altesor, M., and Rodríguez-Seijas, J. (2014). Comprehensive review on lactate metabolism in human health. Mitochondrion *17*, 76–100.

Bellion, A., Baudoin, J.P., Alvarez, C., Bornens, M., and Métin, C. (2005). Nucleokinesis in tangentially migrating neurons comprises two alternating phases: forward migration of the Golgi/centrosome associated with centrosome splitting and myosin contraction at the rear. J. Neurosci. *25*, 5691–5699.

Benson, D.L., Watkins, F.H., Steward, O., and Banker, G. (1994). Characterization of GABAergic neurons in hippocampal cell cultures. J. Neurocytol. *23*, 279–295.

Bertholet, A.M., Millet, A.M., Guillermin, O., Daloyau, M., Davezac, N., Miquel, M.C., and Belenguer, P. (2013). OPA1 loss of function affects in vitro neuronal maturation. Brain *136*, 1518–1533.

Cheng, A., Wan, R., Yang, J.L., Kamimura, N., Son, T.G., Ouyang, X., Luo, Y., Okun, E., and Mattson, M.P. (2012). Involvement of PGC-1α in the formation and maintenance of neuronal dendritic spines. Nat. Commun. *3*, 1250.

Chevallier, J.A., Von Allmen, G.K., and Koenig, M.K. (2014). Seizure semiology and EEG findings in mitochondrial diseases. Epilepsia *55*, 707–712.

Daou, P., Hasan, S., Breitsprecher, D., Baudelet, E., Camoin, L., Audebert, S., Goode, B.L., and Badache, A. (2014). Essential and nonredundant roles for Diaphanous formins in cortical microtubule capture and directed cell migration. Mol. Biol. Cell *25*, 658–668.

Donthamsetty, S., Brahmbhatt, M., Pannu, V., Rida, P.C., Ramarathinam, S., Ogden, A., Cheng, A., Singh, K.K., and Aneja, R. (2014). Mitochondrial genome regulates mitotic fidelity by maintaining centrosomal homeostasis. Cell Cycle *13*, 2056–2063.

Golden, J.A., Zitz, J.C., McFadden, K., and Cepko, C.L. (1997). Cell migration in the developing chick diencephalon. Development *124*, 3525–3533.

Graham, B.H., Waymire, K.G., Cottrell, B., Trounce, I.A., MacGregor, G.R., and Wallace, D.C. (1997). A mouse model for mitochondrial myopathy and cardiomyopathy resulting from a deficiency in the heart/muscle isoform of the adenine nucleotide translocator. Nat. Genet. *16*, 226–234.

Henderson, P.J., and Lardy, H.A. (1970). Bongkrekic acid. An inhibitor of the adenine nucleotide translocase of mitochondria. J. Biol. Chem. *245*, 1319–1326.

Kann, O., Papageorgiou, I.E., and Draguhn, A. (2014). Highly energized inhibitory interneurons are a central element for information processing in cortical networks. J. Cereb. Blood Flow Metab. *34*, 1270–1282.

Khalaf-Nazzal, R., Bruel-Jungerman, E., Rio, J.P., Bureau, J., Irinopoulou, T., Sumia, I., Roumegous, A., Martin, E., Olaso, R., Parras, C., et al. (2013). Organelle and cellular abnormalities associated with hippocampal heterotopia in neonatal doublecortin knockout mice. PLoS ONE *8*, e72622.

Kimura, T., and Murakami, F. (2014). Evidence that dendritic mitochondria negatively regulate dendritic branching in pyramidal neurons in the neocortex. J. Neurosci. *34*, 6938–6951.

Kulka, R.G., and Cooper, C. (1962). The action of oligomycin on the inorganic orthophosphate-adenosine triphosphate and adenosine diphosphate-adenosine triphosphate exchange reactions of digitonin particles. J. Biol. Chem. *237*, 936–939.

Lee, J., Schriner, S.E., and Wallace, D.C. (2009). Adenine nucleotide translocator 1 deficiency increases resistance of mouse brain and neurons to excitotoxic insults. Biochim. Biophys. Acta *1787*, 364–370.

Levy, S.E., Chen, Y.S., Graham, B.H., and Wallace, D.C. (2000). Expression and sequence analysis of the mouse adenine nucleotide translocase 1 and 2 genes. Gene *254*, 57–66.

Lysko, D.E., Putt, M., and Golden, J.A. (2011). SDF1 regulates leading process branching and speed of migrating interneurons. J. Neurosci. *31*, 1739–1745.

Lysko, D.E., Putt, M., and Golden, J.A. (2014). SDF1 reduces interneuron leading process branching through dual regulation of actin and microtubules. J. Neurosci. *34*, 4941–4962.

Marín, O. (2012). Interneuron dysfunction in psychiatric disorders. Nat. Rev. Neurosci. *13*, 107–120.

Marín, O., Valdeolmillos, M., and Moya, F. (2006). Neurons in motion: same principles for different shapes? Trends Neurosci. *29*, 655–661.

Marroquin, L.D., Hynes, J., Dykens, J.A., Jamieson, J.D., and Will, Y. (2007). Circumventing the Crabtree effect: replacing media glucose with galactose increases susceptibility of HepG2 cells to mitochondrial toxicants. Toxicol. Sci. *97*, 539–547.

Nasrallah, M.P., Cho, G., Simonet, J.C., Putt, M.E., Kitamura, K., and Golden, J.A. (2012). Differential effects of a polyalanine tract expansion in Arx on neural development and gene expression. Hum. Mol. Genet. *21*, 1090–1098.

Noctor, S.C., Martínez-Cerdeño, V., Ivic, L., and Kriegstein, A.R. (2004). Cortical neurons arise in symmetric and asymmetric division zones and migrate through specific phases. Nat. Neurosci. *7*, 136–144.

Polleux, F., Whitford, K.L., Dijkhuizen, P.A., Vitalis, T., and Ghosh, A. (2002). Control of cortical interneuron migration by neurotrophins and PI3-kinase signaling. Development *129*, 3147–3160.

Ronchi, J.A., Figueira, T.R., Ravagnani, F.G., Oliveira, H.C., Vercesi, A.E., and Castilho, R.F. (2013). A spontaneous mutation in the nicotinamide nucleotide transhydrogenase gene of C57BL/6J mice results in mitochondrial redox abnormalities. Free Radic. Biol. Med. *63*, 446–456.

Rossignol, D.A., and Frye, R.E. (2012). Mitochondrial dysfunction in autism spectrum disorders: a systematic review and meta-analysis. Mol. Psychiatry *17*, 290–314.

Sapir, T., Frotscher, M., Levy, T., Mandelkow, E.M., and Reiner, O. (2012). Tau's role in the developing brain: implications for intellectual disability. Hum. Mol. Genet. *21*, 1681–1692.

Schaefer, A.M., Taylor, R.W., Turnbull, D.M., and Chinnery, P.F. (2004). The epidemiology of mitochondrial disorders–past, present and future. Biochim. Biophys. Acta *1659*, 115–120.

Shinohara, R., Thumkeo, D., Kamijo, H., Kaneko, N., Sawamoto, K., Watanabe, K., Takebayashi, H., Kiyonari, H., Ishizaki, T., Furuyashiki, T., and Narumiya, S. (2012). A role for mDia, a Rho-regulated actin nucleator, in tangential migration of interneuron precursors. Nat. Neurosci. *15*, 373–380, S371–S372.

Stenman, J., Toresson, H., and Campbell, K. (2003). Identification of two distinct progenitor populations in the lateral ganglionic eminence: implications for striatal and olfactory bulb neurogenesis. J. Neurosci. *23*, 167–174.

Surin, A.M., Khiroug, S., Gorbacheva, L.R., Khodorov, B.I., Pinelis, V.G., and Khiroug, L. (2012). Comparative analysis of cytosolic and mitochondrial ATP synthesis in embryonic and postnatal hippocampal neuronal cultures. Front. Mol. Neurosci. *5*, 102.

Valenti, D., de Bari, L., De Filippis, B., Henrion-Caude, A., and Vacca, R.A. (2014). Mitochondrial dysfunction as a central actor in intellectual disability-related diseases: an overview of Down syndrome, autism, Fragile X and Rett syndrome. Neurosci. Biobehav. Rev. *46*, 202–217.

Wang, L., Ye, X., Zhao, Q., Zhou, Z., Dan, J., Zhu, Y., Chen, Q., and Liu, L. (2014). Drp1 is dispensable for mitochondria biogenesis in induction to pluripotency but required for differentiation of embryonic stem cells. Stem Cells Dev. *23*, 2422–2434.

Yamada, M., Yoshida, Y., Mori, D., Takitoh, T., Kengaku, M., Umeshima, H., Takao, K., Miyakawa, T., Sato, M., Sorimachi, H., et al. (2009). Inhibition of calpain increases LIS1 expression and partially rescues in vivo phenotypes in a mouse model of lissencephaly. Nat. Med. *15*, 1202–1207.